## Ministry of Education TECHNICAL UNIVERSITY OF CIVIL ENGINEERING BUCHAREST

Faculty of Hydrotechnics

## Phd. student Ing. Bogdan-Iulian DOROFTEI

# NUMERICAL CONTRIBUTIONS REGARDING THE INTERACTION OF WIND WITH PERMEABLE OBSTACLES FOR THE PROTECTION OF SANDY SOILS

-DOCTORAL THESIS-- SUMMARY -

Scientific coordinators
Prof. univ. dr. ing. Mircea DEGERATU
Prof. univ. dr. Georgeta BANDOC

Bucharest

2023

### TABLE OF CONTENTS

1.	ANALYSIS OF ENVIRONMENTAL CHARACTERISTICS IN AREAS WITH SANDY SOIL3
1.	1 INTRODUCTION
1.	2 THE SITUATION OF SANDY SOIL DEGRADATION IN ROMANIA
1.	3 STUDYED SOLUTIONS5
1.	4 ELEMENTS OF THEORY ON WHICH THE TAKEN THEME IS BASED5
OBS	NUMERICAL SIMULATION OF AIR MOVEMENT IN THE PRESENCE OF SOME STACLES OF THE TYPE OF PROTECTIVE SCREENS WITH DIFFERENT DEGREES OF EMEABILITY
2.	1 TURBULENCE SCALES
2.	2 NUMERICAL SIMULATIONS FOR THE MODELING OF TURBULENT MOTION
2.	OPTIONS FOR OPTIMAL DIMENSIONING OF THE CALCULATION CELL
2. N	4 PERFORMING THE NUMERICAL SIMULATION IN THE COMSOL MULTIPHYSICS UMERICAL MODELING PROGRAM15
E	.5 NUMERICAL SIMULATIONS OF THE PHENOMENON OF AIR FLOW IN THE XPERIMENTAL VEIN OF THE WIND TUNNEL WITH DISCONTINUITY BY NTRODUCING PROTECTIVE SCREENS INTO THE SYSTEM
	NUMERICAL TESTS FOR WIND EROSION REDUCTION SOLUTIONS UNDER THE FION OF THE WIND21
	1 NUMERICAL MODELING OF AIR MOVEMENT OVER SANDY SOIL PROVIDED //ITH PROTECTIVE SCREENS21
3.	2 RESULTS OF NUMERICAL SIMULATIONS
3.	4. CONCLUSIONS REGARDING THE NUMERICAL TESTS28
4.	CONTRIBUTIONS OF THE THESIS TO THE FIELD OF WIND ENGINEERING31
C	.1. Optimal computational cell sizing for motion domain discretization33
	2.2. Validation (calibration) of the numerical model with the experimental one using RANS and ES numerical simulations
	.3. Creation of a numerical model of air flow over a series of permeable screens based on the reviously validated model
	.4. Performing a series of air flow simulations over a series of permeable screens at a reference ind of various speeds
	2.5. Identifying cases where the velocity downstream of one or more permeable obstacles falls elow the particle entrainment velocity
SEL	ECTIVE BIBLIOGRAPHY36

### 1. ANALYSIS OF ENVIRONMENTAL CHARACTERISTICS IN AREAS WITH SANDY SOIL

The main purpose of this chapter concerns the study of the interaction of sand particles with the wind, in order to establish a link between the characteristics of the solid medium (sand particles) and the characteristics of the fluid medium (air) in motion, which transports the sand by entrainment, thus causing the phenomenon of wind erosion.

#### 1.1 INTRODUCTION

Man's influence on the environment, being very strong in recent centuries, has led to the emergence of a new geological period called the Anthropocene. Period in which man, through his actions, led to the aggravation of some environmental problems, including land degradation.

Land degradation is a serious global environmental problem, given the numerous negative ecological and socio-economic implications. On a global scale, several major regions affected by intense land degradation have been identified, namely the European Mediterranean region, the Sahel, Mesopotamia and the loess region of China. The main environmental problems identified in these regions are related to the physical degradation (water and wind erosion), chemical (salination) and biological (oxidation of organic matter on the soil surface) land, but also the loss / degradation of vegetation (and implicitly the capacity of carbon storage), of the soil's infiltration / water storage capacity, of organic matter, the amplification of dust in the atmosphere, etc.

#### 1.2 THE SITUATION OF SANDY SOIL DEGRADATION IN ROMANIA

One of the causes of soil degradation is wind erosion, and this phenomenon is increasing in areas without high vegetation, especially along agricultural fields, where soil degradation has a devastating impact on crops. The topsoil being gradually removed, it leaves the land barren and unproductive, the plants being unable to develop roots, thus generating a decrease in the production of cereal and vegetable plants. Another effect caused by wind erosion is the raising of dust clouds, this phenomenon, once developed in populated areas, has a harmful impact on the health of the human body due to the inhalation of dust particles by people. These non-organic particles, once inhaled, can cause health problems in the lungs but also on other organs such as the brain or liver when the smaller particles are dissolved in the blood. Clouds of dust can also affect transport, suspended particles in the vicinity of an airport or a highway can make visibility difficult and sometimes even make vehicles unable to move due to damage to their engines or fuselage. Erosion represents a negative socio-economic impact on the area affected by this phenomenon, which leads to different studies for control methods of its effect.

In Romania, the south of Oltenia is recognized at national level for the current accentuated stage of land degradation, against the background of a long synergy of regional climate changes, restrictive hydrological, pedological and ecological conditions, respectively of anthropic pressures on land use/cover.

The situation of sandy lands in Romania according to the areas occupied by them [km<sup>2</sup>]

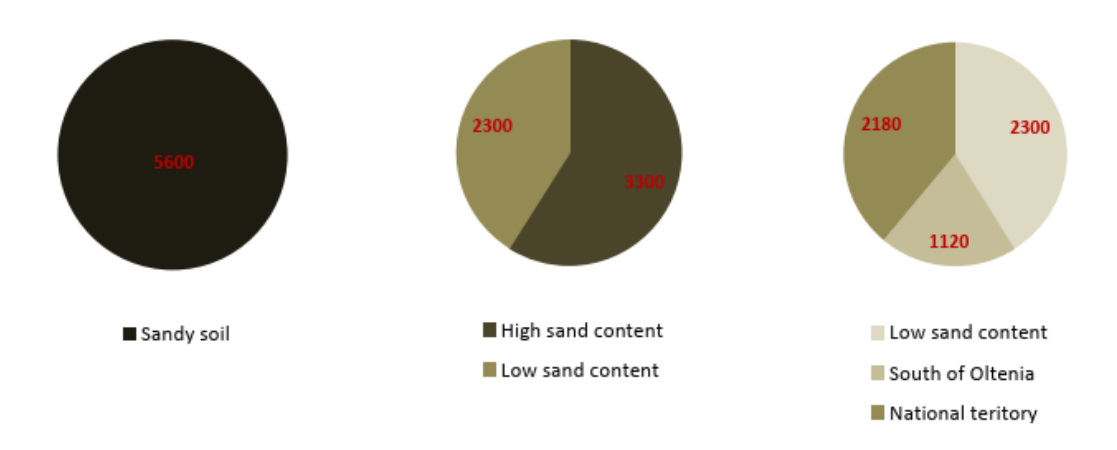


Fig. 1.2.1 - The distribution of sandy soils on the territory of Romania

It can be observed that out of the total of 5600 km<sup>2</sup> of sandy soil existing on the territory of the country, only 3300 km<sup>2</sup> are soils with a very high sand content (those with a sandy and sandy texture), and of these only 1120 km<sup>2</sup> are found in the south of Oltenia. Thus, it can be considered that 20% of the sandy soils on the territory of the country are found in the southern area, in Oltenia (SRCS; 1980).

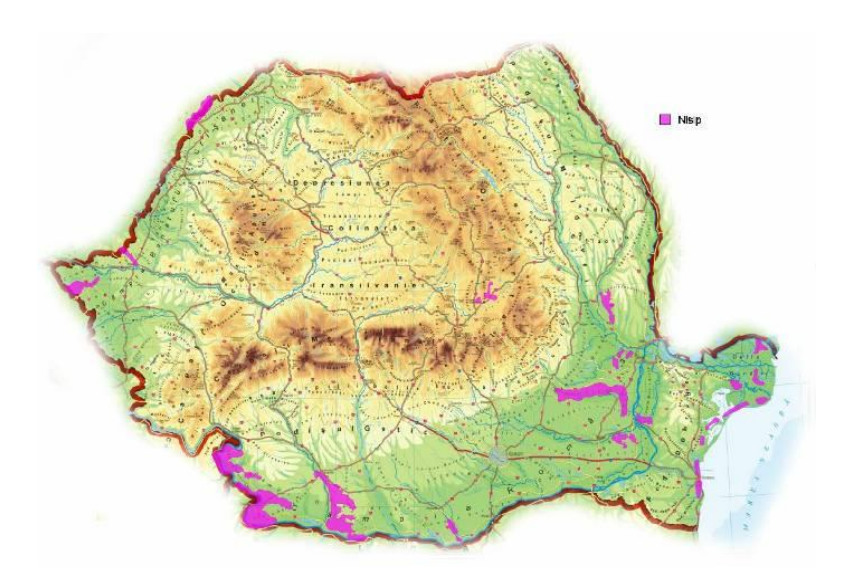


Fig. 1.2.2 - Map of the spread of sandy soils in Romania

Sandy soils and sands appear dispersed in perimeters of different sizes within several geomorphological units (Fig. 1.2.2). Regarding the distribution by counties, the largest stretches of sand and sandy soils with agricultural use appear in the counties of Dolj, Mehedinţi, Tulcea, Brăila, Satu Mare and Galati.

#### 1.3 STUDYED SOLUTIONS

One of the ways to reduce the phenomenon of erosion is by using protective screens located in the direction of wind flow, in areas strongly affected by wind erosion of soils, to reduce the speed of the air, which drives the fine sand particles. An important tool in the act of creating protective screens is the use of a cartographic and statistical database on the wind regime. To establish a calculation model from which to build these barriers, it was first necessary to study the fluid-solid polyphase flow that drives the solid particles, thus displacing them and causing the erosion effect. Thus, an analysis of the environmental characteristics of sandy land areas was carried out as a starting point for the present research topic.

#### 1.4 ELEMENTS OF THEORY ON WHICH THE TAKEN THEME IS BASED

Air is a transport medium for fine particles, at its high speeds the particles can be bigger and bigger, and the area of effect of this transport can be bigger and bigger. Thus arises the phenomenon of soil erosion through the action of air, wind erosion.

#### 1.4.1 Entrainment of solid particles in motion

As long as the velocity of the fluid current remains below a certain threshold, the solid particle remains at rest. When that limit is exceeded, the particle starts moving, and is driven through one of the three modes of transport (Fig. 1.4.8):

- tumbleing
- slow lifting from the ground
- suspension

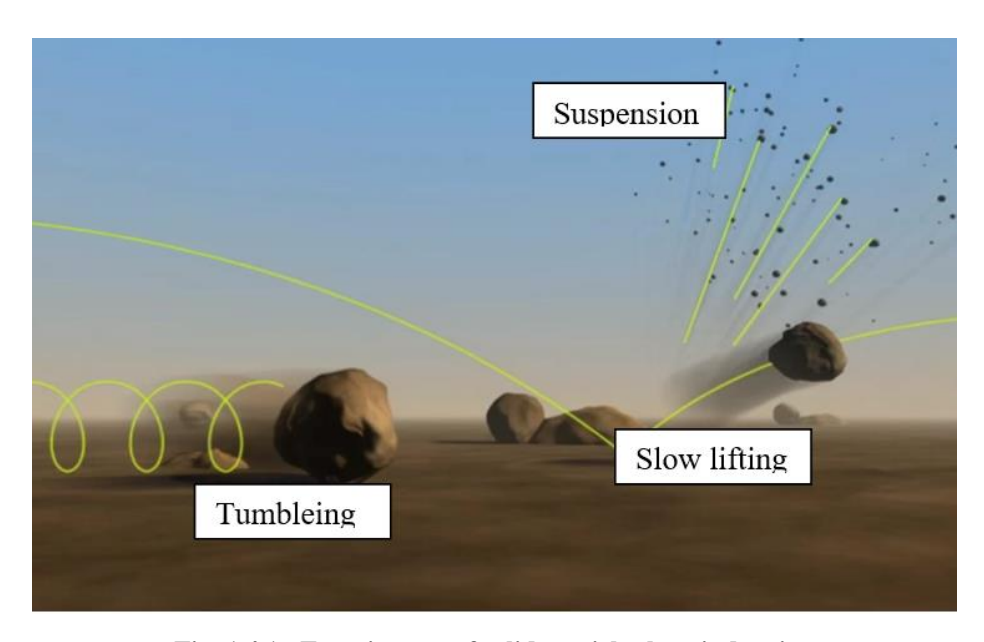


Fig. 1.4.1 - Entrainment of solid particles by wind action

As the fluid speed increases, the particle begins to move in jumps whose frequency, amplitude and length increase with the speed of the current. Due to the fact that the resultant of the dynamic pressure forces that the fluid stream exerts on the particle does not pass through its center of gravity, a moment appears that causes the particle to rotate between the jump points. The rotation of the solid

particle in the fluid stream produces a Magnus effect which, combined with the reflection of the grain at the points of impact, changes its trajectory. When the velocity pulsations exceed certain values, the particles are moved into suspension.

#### 1.4.2 Wind action on sand particles

Petrov M.P. (1986), consider that the sand begins to move when the wind speed at the sand surface is greater than 3.5...4.5 m/s, and the grains that begin to move have a diameter of 0.25...0, 01 mm. Molinkov quoted by Moţoc M. (1963) mentions that at speeds of 0.5...3.5 m/s the wind does not entrain soil particles. The author's results are listed in Table 4.3. Also in this table are the values developed by Sokolov M.I. (1884).

Table 1.4.1 - Entrainment velocit	v values of san	d particles as a	function of grain	ı diameter

Author	Localization	Speed [m/s]	Diameter os sand particle [mm]
Petrov M.P.	On the surface of sand	3,54,5	0,010,25
		47	0,5<
Molinkov		711	0,501,00
IVIOIIIIKOV	-	1127	12
		1728	25
Sokolov M.I.	Soil surface	3,56,7	0,100,25
SUKUIUV IVI.I.	Sull sullace	11,413	12

Canarache (1990), analyzing the granulometric fractions collected at the height of the soil surface with the help of a device specially built for their capture, found that in the range of 10...160 cm the coarse sand is in a proportion of 20...22%, with the sand fine 70% and physical clay 8...10%. From the height of 160 cm, the amount of coarse sand begins to decrease and the amount of fine sand increases, physical and colloidal clay remaining almost constant.

The flow rate or flow rate expressed in mg/cm<sup>2</sup>/s is the most intense in the first 2.5 cm, both for particles moved in jumps and for particles carried in suspension. Then as we rise above the ground up to 60 cm the flows decrease; much faster those carried in jumps and slower those carried in suspension.

From the point of view of the type of soils, the most strongly exposed to wind erosion are "sands" then "sandy loams" and finally "heavy clays".

The reduction, up to the complete annihilation of the erosion phenomena of the sand layer, depends on local factors such as the wind, the roughness of the sandy terrain, the distance between the forest curtains (L), etc., factors that are difficult to control. For these reasons, the results of experimental determinations, on a natural scale, carried out by various researchers, differ from one place to another, from researcher to researcher, from country to country, they contribute to the existence of differences in the dimensioning of constructive elements.

## The distance between two forest curtains placed successively in different countries according to Van der Linde

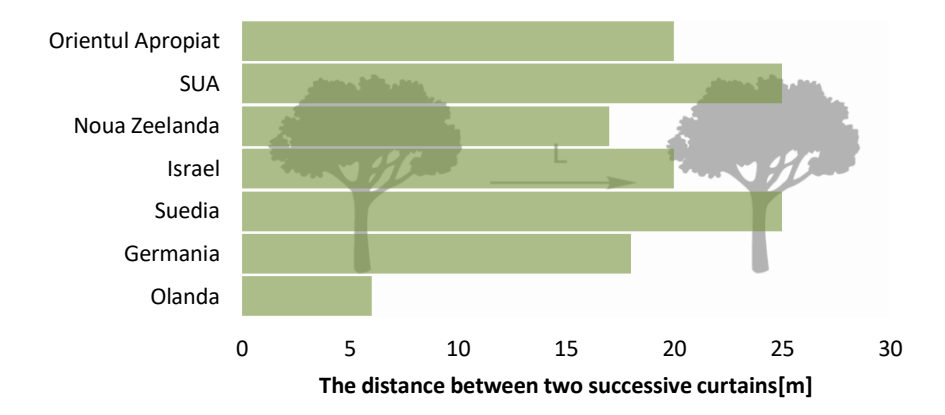


Fig. 1.4.2 - Recommendation for setting up successive forest curtains

## 2. NUMERICAL SIMULATION OF AIR MOVEMENT IN THE PRESENCE OF SOME OBSTACLES OF THE TYPE OF PROTECTIVE SCREENS WITH DIFFERENT DEGREES OF PERMEABILITY

#### 2.1 TURBULENCE SCALES

Energy is transferred (dissipated) from large structures (the energy contained in structures of a certain scale) to the smallest structures of turbulence (Kolmogorov's theory, 1941).

A region of the turbulent flow of size l, which can be identified as having a coherent presentation, can be shown and introduced as a turbulent structure.

A turbulent structure of a given size may contain other structures of smaller size, and may be. in her turn. contained in a larger-scale turbulent structure.

In addition to the length scale l, we should also mention the speed scales  $u_l$  and time scales  $\tau_l$ , which are in the obvious relationship:

$$\tau_l = l/u_l \tag{2.1}$$

#### 2.2 NUMERICAL SIMULATIONS FOR THE MODELING OF TURBULENT MOTION

The partial differential equations governing the motion of real fluids are solved numerically and represented by numerical treatment of fluid dynamics (CFD simulations). These numerical simulations deal with the problem of turbulent flow.

Advances related to the development of numerical methods and the creation of algorithms to implement these methods directly depend on the continued development of computer-aided computing (referring here to both the hardware-related capability of a computer and the software-related capability).

In the last decades, progress has been substantial in this branch, the main obstacle in CFD remaining the turbulence of fluid motion, namely the specification of Reynolds stresses, compared to the theoretical treatment of flow problems solved by time-averaged Navier-Stokes equations.

The following paragraphs present the known methods of "closing" the Navier-Stokes equations, for various averaging orders, noting that a more accurate solution involves avoiding this problem and searching for the solutions of the unmediated Navier-Stokes equations.

Three types of simulations can be used for numerical modeling of turbulent motion<sup>1</sup>:

Direct numerical simulation (Direct Numerical Solution - DNS) which allows solving all fluctuations in the flow provided that the discretization of the model is very fine and the time steps (time discretization) are very small. These two conditions become increasingly important as the Reynold number increases, and this can slow down the computer-aided calculation process with which the modeling is performed..

Reynolds Averaged Navier-Stokes simulations (Reynolds Averaged Navier-Stokes - RANS) are the most common types of modeling used in engineering and by researchers. These simulations introduce a new set of unknowns, called the Reynolds stresses that must be additionally modeled to close the equations of motion.

Simulations with macroscopic units<sup>2</sup> (Large Eddy Simulations - LES), are placed between DNS and RANS simulations in terms of computational processing requirements. These types of simulations must be performed on a three-dimensional geometric model in which the large eddies (Large Eddy) that appear in the fluid flow are resolved. Spatial filter models (Sub Grid Scale - SGS) will be applied to resolve small eddies. Thus, LES simulations do not require as much processing capacity as DNS ones and implicitly the discretization of the domain will not be as fine.

It is also worth mentioning the hybrid model for the simulation of detached macroscopic units (Detached Eddy Simulation - DES), which is a combination of LES and RANS, where the contact zone between a solid surface and fluid is solved according to a RANS simulation and the flow of the fluid outside the zone of influence of this type of interaction is solved as an LES simulation.

#### 2.3 OPTIONS FOR OPTIMAL DIMENSIONING OF THE CALCULATION CELL

To avoid numerical modeling in DNS and overcrowding the computational process of solving the problem, the discretization of the numerically modeled motion domain must be sparse enough that the computational cell has a physical size larger than the Kolmogorov length scale to prevent modeling of small eddies. At the same time, the cell will have to be dimensioned to be able to include the large eddies that will be resolved by the LES simulation.

To determine the Kolmogorov length, 2 options were used, presented below.

<sup>&</sup>lt;sup>1</sup> http://imechanica.org/files/fluent\_13.0\_lecture06-turbulence.pdf

<sup>&</sup>lt;sup>2</sup> McComb W.D. *Turbulenta fluidelor (The Physics of Fluid Turbulence* in Oxford University Press) tradus de Savulescu N. St. 1997, in ed. Tehnica, Bucuresti

#### 2.3.1 Option 1 - based on Kolmogorov's theory

Kolmogorov's theory (1941) describes how turbulent energy is transferred from large structures to smaller structures of turbulence, the energy contained by structures of a given scale, and how much energy is dissipated by structures of a given scale.

The Kolmogorov hypothesis of local isotropy holds that, in flows with sufficiently large Reynolds numbers, structures with a sufficiently small scale ( $l \ll L$ ) are statistically isotropic, while larger-scale turbulent structures remain anisotropic, L representing the characteristic length of the flow.

According to Kolmogorov's theory, the governing parameters of small-scale turbulent structures are at least the unit energy dissipation rate  $\varepsilon$  (m<sup>2</sup>/s<sup>3</sup>) and the kinematic viscosity v (m<sup>2</sup>/s)

Using these fundamental parameters, one obtains the following relation for the Kolmogorov length scale:

$$\eta = (\nu^3/\varepsilon)^{1/4} \tag{2.19}$$

where the unit energy dissipation rate, equal to the unit energy supply rate has the following expression<sup>3</sup>:

$$\varepsilon = \frac{u_0^3}{L} \tag{2.20}$$

where:

 $u_0$  - the characteristic speed, which is of the order of magnitude of the speed  $u_{rms}$ ;

L - the height of the entrance section to the experimental area.

The following expression will be used to calculate the root mean square of the velocity pulsation:

$$u_{rms} = UI (2.21)$$

where:

 $u_{rms}$  - root mean square deviation of velocity pulsation;

*I* - initial turbulent intensity;

U - the magnitude of the initial velocity.

Using the relations (2.19) - (2.21) one can establish the Kolmogorov length scale, corresponding to the dimensions of very small vortices. The choice of computational cell will be made for a size 6 to 30 times larger than the Kolmogorov length scale to model only the large eddies, specific to LES simulations<sup>4</sup>.

\_

<sup>&</sup>lt;sup>3</sup> McComb W.D. *Turbulenta fluidelor (The Physics of Fluid Turbulence* in Oxford University Press) tradus de Savulescu N. St. 1997, in ed. Tehnica, Bucuresti

<sup>&</sup>lt;sup>4</sup> https://www.researchgate.net/profile/Chitrarth\_Lav

#### 2.3.2 Option 2 - based on full-scale TKE model

In Computational Fluid Mechanics (CFD) it is impossible to numerically simulate turbulence without discretizing the domain with cell dimensions of the size of the Kolmogorov length scale. This will make the simulation DNS-type, which will overload the memory and computing power of the computers, thus resorting to the use of different types of numerical turbulence models. These models simulate the effect of turbulence, and one of them is called Turbulent Kinetic Energy (TKE).

The exact method of solving the TKE model depends on the turbulence model used. For example, the k- $\varepsilon$  model assumes turbulence isotropy. This assumption makes the modeling of the turbulence quantities (k and  $\varepsilon$ ) more simplistic, but will not yield in situations where the turbulence has an anisotropic character<sup>5</sup>.

The TKE model can be quantified by turbulent kinetic energy:

$$k = \frac{1}{2} \left[ \overline{(u')^2} + \overline{(v')^2} + \overline{(w')^2} \right]$$
 (2.22)

TKE can be produced by fluid stresses, friction, buoyancy forces, or due to external forces at low-frequency turbulence scales (integral scale). The kinetic energy of the turbulence is then transferred to the fluid from near to near and is dissipated by viscous forces when they reach the Kolmogorov length scale. This process of production, transport and dissipation has the following expression<sup>6</sup>:

$$\frac{Dk}{Dt} + \nabla \cdot T' = P - \varepsilon \tag{2.23}$$

where:

 $\frac{Dk}{Dt}$  - the material derivative (substantial derivative) of the TKE flow;

 $\nabla \cdot T'$  - turbulent transport of TKE

P – production of TKE

 $\varepsilon$  - dissipation of TKE

Assuming that the density and viscosity are constant, the form of the TKE equations is as follows:

$$\frac{\partial k}{\partial t} + \overline{u_j} \frac{\partial k}{\partial x_j} = -\frac{1}{\rho} \frac{\partial \overline{u_i' p'}}{\partial x_i} - \frac{1}{2} \frac{\partial \overline{u_j' u_j' u_i'}}{\partial x_i} + \nu \frac{\partial^2 k}{\partial x_j^2} - \overline{u_i' u_j'} \frac{\partial \overline{u_i}}{\partial x_j} - \nu \frac{\overline{\partial u_i'}}{\partial x_j} \frac{\partial \overline{u_i'}}{\partial x_j} - \frac{g}{\rho} \overline{\rho' u_i'} \delta_{i\varepsilon}$$
(2.24)

<sup>&</sup>lt;sup>5</sup> Laurence, D. (2002). "Applications of Reynolds Averaged Navier Stokes Equations to Industrial Flows". In van Beeck, J. P. A. J.; Benocci, C. Introduction to Turbulence Modelling, Held March 18–22, 2002 at Von Karman Institute for Fluid Dynamics. Sint-Genesius-Rode: Von Karman Institute for Fluid Dynamics

<sup>&</sup>lt;sup>6</sup> Pope, S. B. (2000). Turbulent Flows. Cambridge: Cambridge University Press

where:

- 1 local derivative;
- 2 advection;
- 3 pressure diffusion;
- 4 turbulence transport (T);
- 5 viscous molecular transport;
- 6 production (P);
- 7 dissipation ( $\epsilon$ );
- 8 buoyancy.

To find out the TKE energy dissipation, the following equations are proposed<sup>7</sup>:

$$k = \frac{3}{2}(UI)^2 \tag{2.25}$$

where:

*I* - initial turbulent intensity;

U - the magnitude of the initial velocity.

$$\varepsilon = c_u^{\frac{3}{2}} k^{\frac{3}{2}} l^{-1} \tag{2.26}$$

where:

*l* - turbulence length scale;

 $c_{\mu}$  - coefficient with the usual value of 0.09.

$$I = 0.16Re^{-\frac{1}{8}} \tag{2.27}$$

The turbulence length scale can be estimated as follows:

$$l = 0.07L (2.28)$$

<sup>7</sup> Laurence, D. (2002). "Applications of Reynolds Averaged Navier Stokes Equations to Industrial Flows". In van Beeck, J. P. A. J.; Benocci, C. Introduction to Turbulence Modelling, Held March 18–22, 2002 at Von Karman Institute for Fluid Dynamics. Sint-Genesius-Rode: Von Karman Institute for Fluid Dynamics. Pope, S. B. (2000). Turbulent Flows. Cambridge: Cambridge University Press. Flórez Orrego; et al. (2012). "Experimental and CFD study of a single phase cone-shaped helical coiled heat exchanger: an empirical correlation". Proceedings of ECOS 2012 – The 25th International Conference on Efficiency, Cost, Optimization, Simulation and Environmental Impact of Energy Systems, June 26–29, 2012, Perugia, Italy. ISBN 978-88-6655-322-9. Boussinesq, J. V. (1877). "Théorie de l'Écoulement Tourbillant". Mem. Présentés par Divers Savants Acad. Sci. Inst. Fr. 23: 46–50. Baldocchi, D. (2005), Lecture 16, Wind and Turbulence, Part 1, Surface Boundary Layer: Theory and Principles, Ecosystem Science Division, Department of Environmental Science, Policy and Management, University of California, Berkeley, CA: USA. https://en.wikipedia.org/wiki/Turbulence\_kinetic\_energy

where:

L - characteristic length.

$$\eta = (\nu^3/\varepsilon)^{1/4} \tag{2.29}$$

Using the relations (2.25) - (2.29) one can establish the Kolmogorov length scale, corresponding to the dimensions of very small vortices. The choice of computational cell will be made for a size 6 to 30 times larger than the Kolmogorov length scale to model only the large eddies, specific to LES simulations<sup>8</sup>.

#### 2.3.3 Numerically modeled motion domain and determination of the Kolmogorov length scale

Next, numerical simulations were carried out in order to model the air movement in the experimental vein of the wind tunnel with discontinuity TAD located in the Laboratory of Aerodynamics and Wind Engineering of the Technical University of Construction Bucharest, whose geometric dimensions are represented in the following figure (Fig. 2.3.1):

#### 2.3.4 Geometry of the modeled range of motion and its characteristics

The area of interest, whose movement was modeled numerically, is called the "Experimental Area", having the dimensions in mm:  $1600 \times 200 \times 400$ ,  $200 \times 400$ , mm being the height of the experimental vein (Fig. 2.3.1).

The experimental area is fed at its upper part by a profiled mixer with a section of  $100 \times 400$  mm, 100 mm being the height of the exit section from the mixer (Fig. 2.3.1).

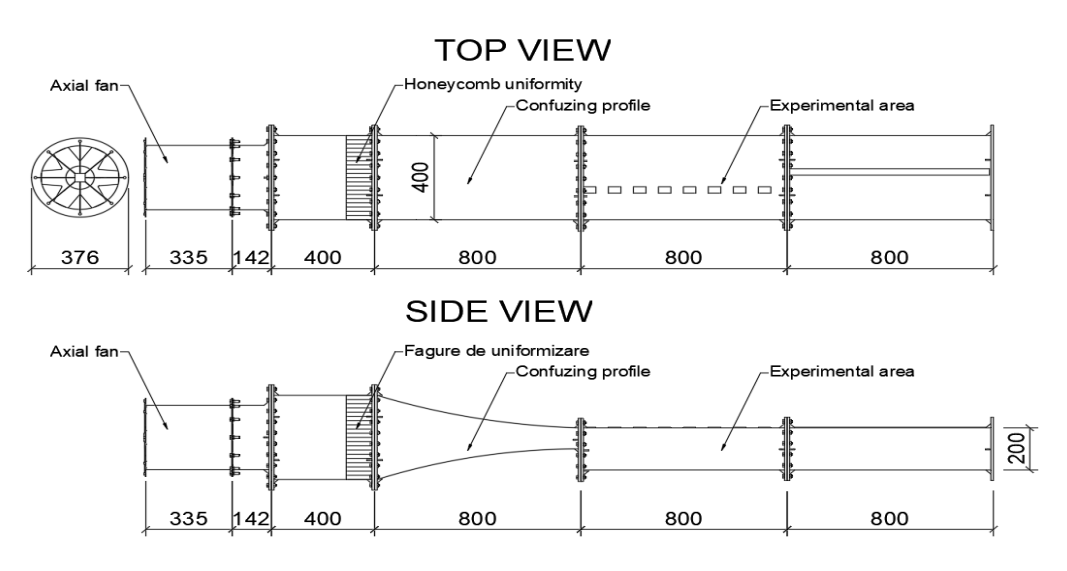


Fig. 2.3.1 - The geometric dimensions of the wind tunnel with discontinuity (TAD)

The air speed at the entrance to the experimental area (the air speed in the exit section of the mixer) can be considered constant on the section and equal to U = 17 m/s, the kinematic viscosity of the air is v = 1.5 10-5 m<sup>2</sup>/s, and the length characteristic is L = 0.1 m, being equal to the height of the exit section from the mixer, in turn equal to the height of the expansion stage.

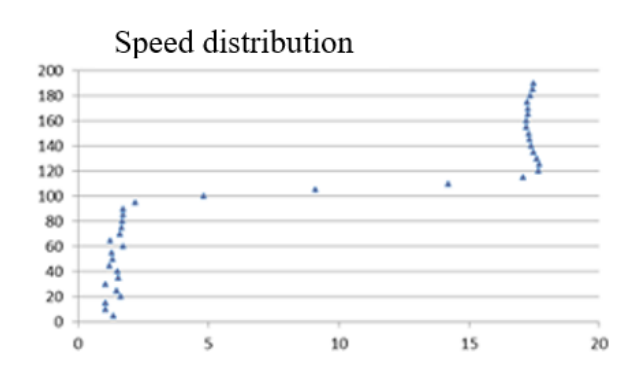
\_

<sup>&</sup>lt;sup>8</sup> https://www.researchgate.net/profile/Chitrarth\_Lav

#### 2.3.5 Calculation of the Kolmogorov length scale according to option 1

According to the measurements in the wind tunnel with discontinuity, in the section entering the experimental vein (Fig. 2.3.2) regarding the velocity and turbulent intensity distributions, a uniform velocity distribution was considered, namely U = 17 m/s, as well as a uniform distribution of the turbulent intensity  $I = 0.02^9$ .

According to the experimental tests carried out in the tunnel, in the entrance section the following values were obtained for the mean velocity and turbulent intensity distributions represented in the figure below:



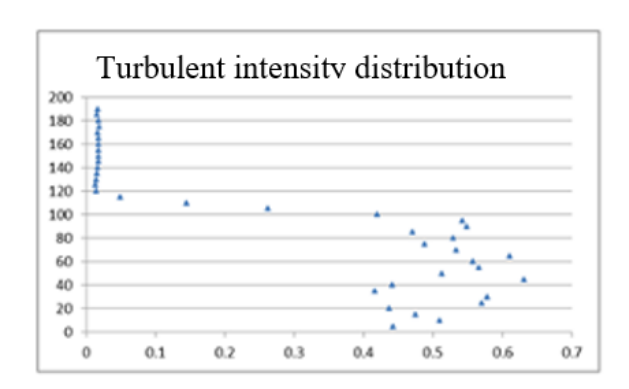


Fig. 2.3.2 - Results of experimental measurements in the section at the entrance to the experimental area of the wind tunnel with discontinuity

According to the expressions (2.19) - (2.21), the values of the characteristic quantities are as follows:

$$u_{rms} = UI = 17 \cdot 0.02 = 0.34 \text{ m/s}$$

$$\varepsilon = \frac{u_{rms}^3}{L} = \frac{0.34^3}{0.1} = 0.4 \text{ m}^2/\text{s}^3$$

$$\eta = \left(\frac{v^3}{\varepsilon}\right)^{\frac{1}{4}} = ((1.5 \cdot 10^{-5})^3 / 0.4)^{1/4} = 0.00030 \text{ m}$$

#### 2.3.6 Calculation of the Kolmogorov length scale according to option 2

Using the initial velocity value mentioned above, equations (2.25) - (2.28) were solved to find the TKE dissipation value, which was inserted into equation (2.29) to calculate the Kolmogorov length scale.

$$L = 0.1 \text{ m}$$

$$Re = \frac{UL}{v} = \frac{17 \cdot 0.1}{1.5 \cdot 10^{-5}} = 1133333.33$$

$$l = 0.07L = 0.07 \cdot 0.1 = 0.007 \text{ m}$$

<sup>&</sup>lt;sup>9</sup> Vladuț C. V. *Modelarea numerică și experimentală a mișcărilor atmosferice la scară medie peste insula Bolund*, Teza de doctorat, 2015, București

$$I = 0.16Re^{-\frac{1}{8}} = 0.16 \cdot 113333.33^{-\frac{1}{8}} = 0.038$$

$$k = \frac{3}{2}(UI)^2 = \frac{3}{2}(17 \cdot 0.038)^2 = 0.63 \text{ m}^4/\text{s}^3$$

$$\varepsilon = C_{\mu}^{\frac{3}{4}}k^{\frac{3}{2}}l^{-1} = 0.09^{\frac{3}{4}} \cdot 0.63^{\frac{3}{2}} \cdot 0.007^{-1} = 11.82 \text{ m}^2/\text{s}^3$$

$$\eta = \left(\frac{v^3}{\varepsilon}\right)^{\frac{1}{4}} = ((1.5 \cdot 10^{-5})^3/11.82)^{1/4} = 0.00015 \text{ m}$$

Note: the difference between the value of the Kolmogorov length scale calculated with option 1 and the value calculated with option 2 is due to the different way of calculating the dissipation rate of unit turbulent energy  $\varepsilon$ .

#### 2.3.7 Choice of cell size with respect to the Kolmogorov length scale

To carry out the LES simulation, a cell will be chosen with a size between the limits of the values found in the practice of numerical simulations, i.e. 6 times to 30 times larger than the Kolmogorov length scale<sup>10</sup>.

Another recommendation is to apply a factor on the Kolmogorov length scale, with a minimum value of 3. This prevents a DNS simulation of the type of finding the statistical properties of the inertial range, which has as its defining element the dimensioning of the cell  $\Delta x \leq 3\eta^{11}$ .

To carry out the LES simulation, a cell will be chosen with a size between the limits of values 6 times to 30 times greater than the Kolmogorov length scale, because it conveys an information from the practice of numerical simulations.

In the case of the previously obtained results for the Kolmogorov length scale, this calculation cell size range is between 0.3 mm x 6 = 1.80 mm and 0.3 mm x 30 = 9.00 mm for variant 1 and between 0,15 mm x 6 = 0.9 mm and 0.15 mm x 30 = 4.5 mm for variant 2. These ranges, corresponding to the two variants of the Kolmogorov length scale calculation, also verify the recommendation that the size of the calculation cell  $\Delta x$  be greater than  $3\eta$  (between  $3 \times 0.15$  mm = 0.45 mm and  $3 \times 0.3$  mm = 0.9 mm).

The graphic representation of the conclusion can be seen in the following figure (Fig. 2.3.3):

-

<sup>&</sup>lt;sup>10</sup> https://www.researchgate.net/profile/Chitrarth\_Lav

<sup>&</sup>lt;sup>11</sup> Kurien S., Taylor M.A., 2005. *Direct Numerical Simulations of Turbulence-Data Generation and Statistical Analysis*, în: Los Alamos Science, vol. 29, pp. 142-151

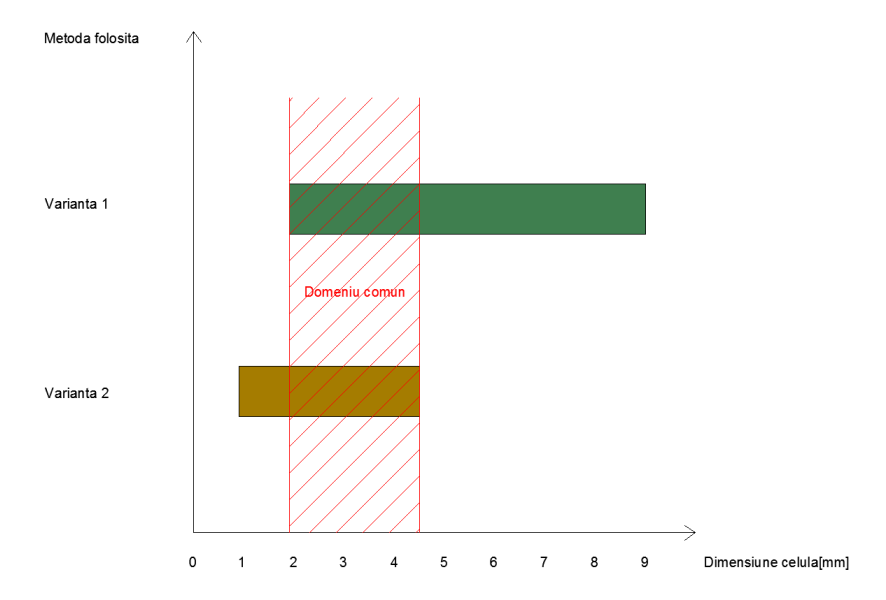


Fig. 2.3.3 - The results of cell sizing according to the 2 variants

Therefore, from the overlap of the domains corresponding to variants 1 and 2 and from the recommendations in practice, it follows that the common domain of the calculation cell size is between 1.8 mm and 4.5 mm.

### 2.4 PERFORMING THE NUMERICAL SIMULATION IN THE COMSOL MULTIPHYSICS NUMERICAL MODELING PROGRAM

Similar to the previously mentioned model, by means of the numerical modeling program COMSOL Multiphysics, a numerical simulation of the physical experiment in the wind tunnel with discontinuity was carried out. The results obtained from the numerical simulation were compared with those obtained from the physical experiment for fitting the model, then compared with the results obtained in the simulation using the LES method.

The numerical calculation using the k- $\varepsilon$  method was carried out by the two-dimensional simulation of the experimental vein of the wind tunnel with discontinuity, having the dimensions of the height of 200 mm and the length of 1600 mm.

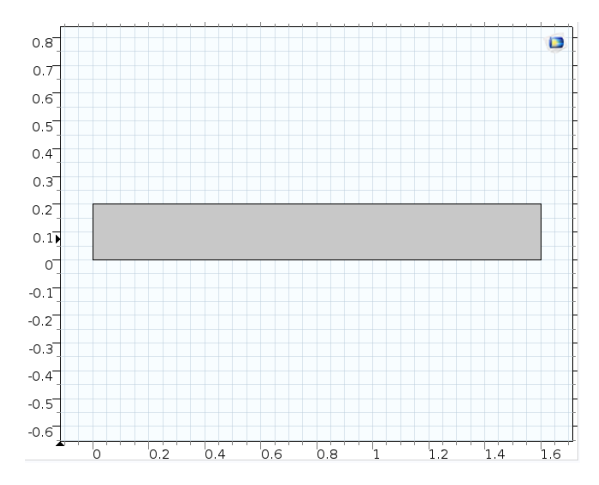
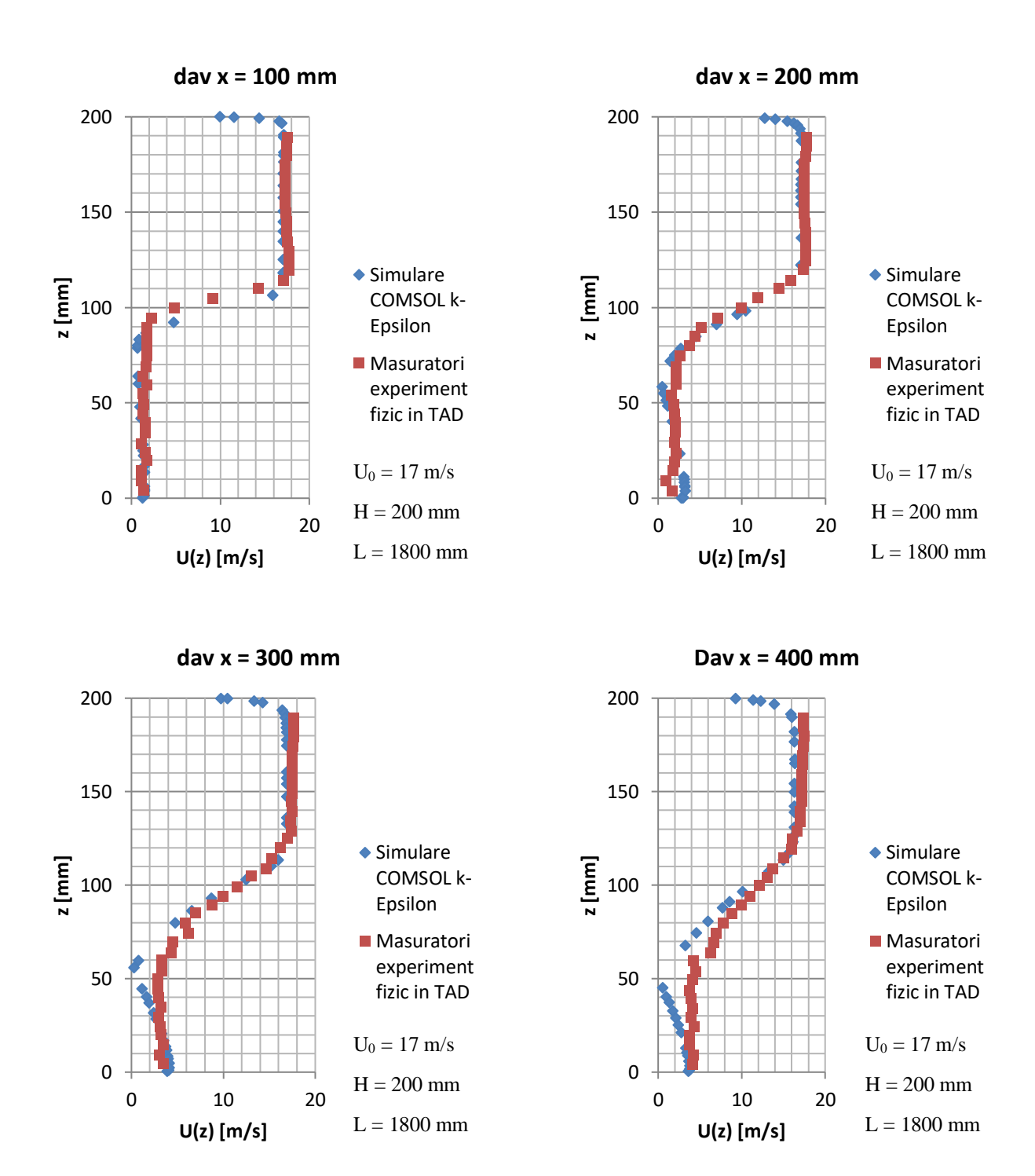
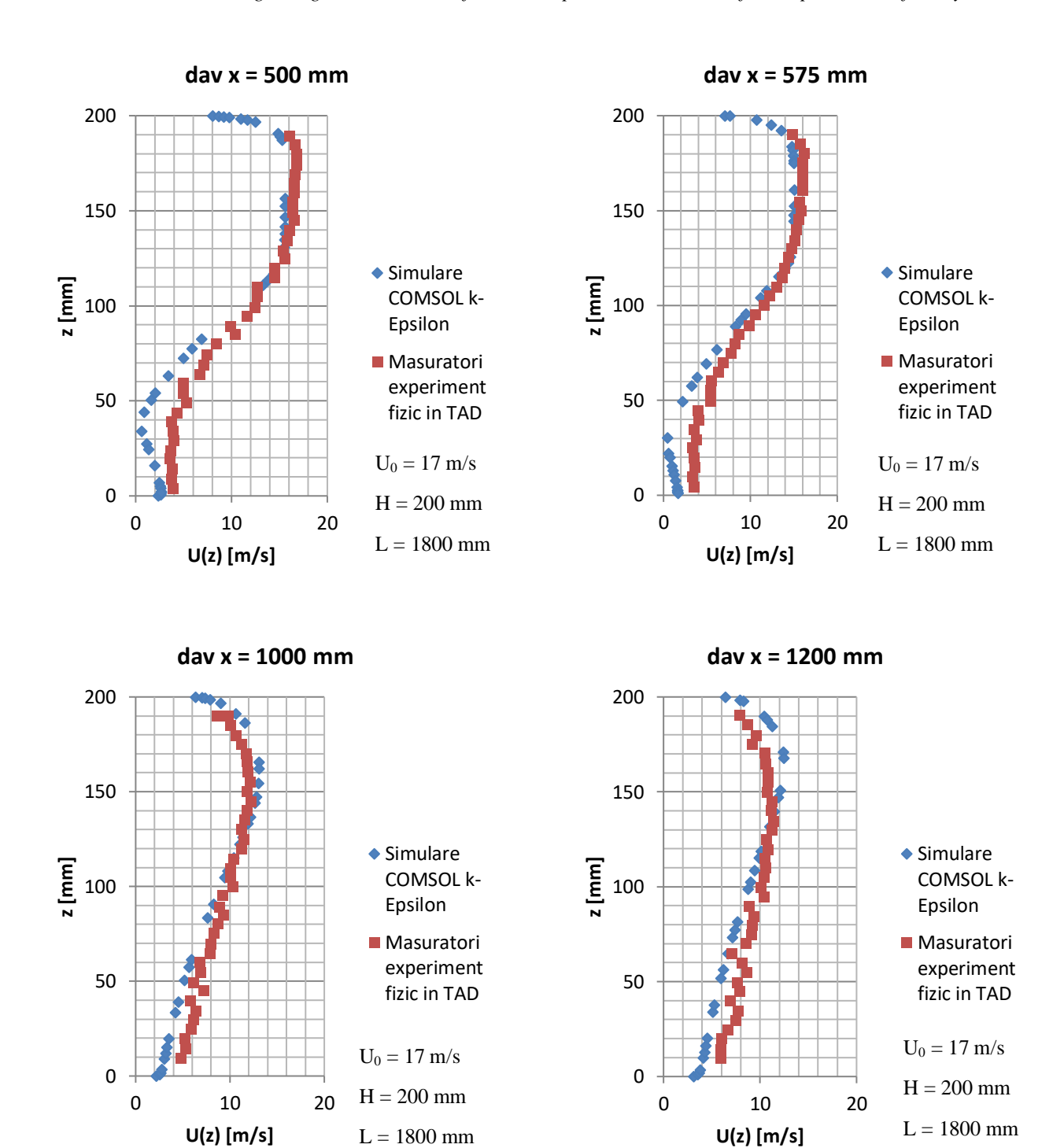
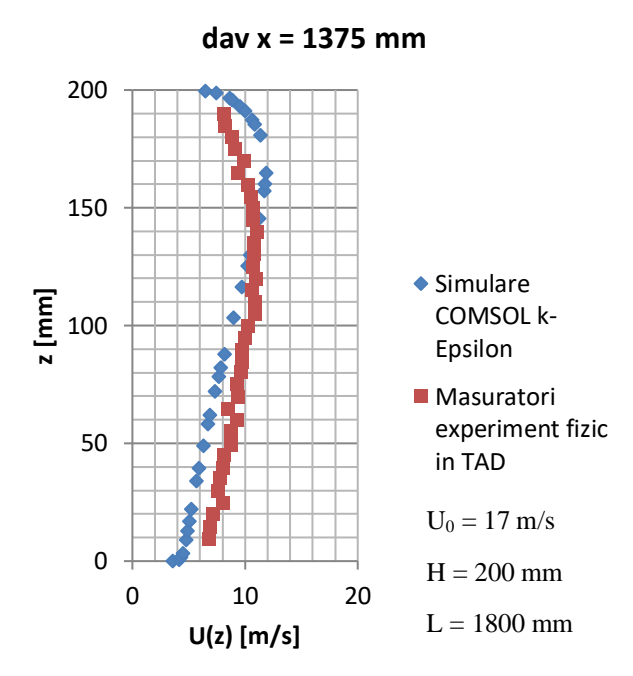


Fig. 2.4.1 – The geometry of the computational domain

- 2.4.1 Simulations and comparisons between velocity intensity determination methods. Validation of the numerical models used
- 2.4.1.1 Comparison of mean velocity profiles in sections  $x=100,\,200,\,300,\,400,\,500,\,575,\,1000,\,1200,\,1375$  mm from the TAD vein obtained by COMSOL k- $\epsilon$  numerical simulation and experimental tests







#### **Results:**

The comparisons of the velocity profiles shown in the previous graphs were obtained by numerical  $k - \varepsilon$  simulation in the finite element modeling program COMSOL Multiphysics<sup>TM</sup> and experimental tests performed in the discontinuity wind tunnel (TAD). The measurements were performed with the Pitot-Prandtl probe, connected to a piezoelectric differential pressure transducer.

On the abscissa you can find the values for the real speed, and on the ordinate the values for the height at which the respective speed was recorded.

It can be seen that the profiles overlap to a very large extent, which leads to the validation of a very good match, regarding the results, between the experiment carried out by numerical modeling and the physical experiment carried out in the wind tunnel with discontinuity.

## 2.5 NUMERICAL SIMULATIONS OF THE PHENOMENON OF AIR FLOW IN THE EXPERIMENTAL VEIN OF THE WIND TUNNEL WITH DISCONTINUITY BY INTRODUCING PROTECTIVE SCREENS INTO THE SYSTEM

After carrying out the numerical simulation of the flow in the wind tunnel with discontinuity and implicitly fitting the numerical model to the physical one, it was proposed to introduce protective screens into the calculation field.

They will have the role of reducing the wind speed in the immediate vicinity of the ground, which means reducing the entrainment of suspended matter.

#### 2.5.1 Selection of Type 1 protective screen characteristics for the numerical experiment

A permeable obstacle was used to model the protective screen inside the tunnel. This boundary condition will be assigned to a segment located inside the simulated tunnel.

The protective screen is of the distributed perforation "wire gauze" type and can be modeled as an edge condition. This allows for an economical implementation of the screen, where the details of the

obstacle do not have to be resolved. The general influence of the shield on the flow field is a loss of the momentum component, a change in the direction of the wind flow, an attenuation of the turbulent kinetic energy and a preservation of the turbulent length scale.

The COMSOL Multiphysics<sup>TM</sup> calculation model requires input of parameters:

*K* - screen resistance;

 $\sigma_s$  - solidity (the ratio between the blocked area and the total area of the screen);

$$K = 0.98 \times ((1 - \sigma_s)^{-2} - 1)^{1.09} \tag{2.30}$$

 $\eta$  - the refractive index;

$$\eta = \sqrt{\frac{K^2}{16} + 1} - \frac{K}{4} \tag{2.31}$$

To choose the optimal parameters of the protective screen, it was taken into account that the *dav* of the experimental vein should not be blocked on a percentage greater than 10% of it.

Thus, a sieve was chosen, used as a protective screen, with the wire diameter d = 0.08 mm and the length and width of the gap  $d_{ochi} = 0.13$  mm.

The free area, which represents the permeability of the screen, was calculated with the following formula:

$$A_{liber\check{a}} = \frac{d_{ochi}^2}{(d_{ochi} + \frac{d}{2})^2} = 0,58$$
 (2.32)

The area of the experimental vein of the wind tunnel with the width of the tunnel  $l_{\text{runel}} = 400 \text{ mm}$  and the height of the tunnel  $h_{\text{tunel}} = 200 \text{ mm}$  was calculated with the following formula:

$$A_{ven\check{a}} = l_{tunel} \times h_{tunel} = 0.08m^2 \tag{2.33}$$

The permeability of the experimental vein section of the wind tunnel, taking into account the 10% passage restriction is as follows:

$$A_{permeabil}^{10\%} = 0.9 \times A_{ven\check{a}} = 0.072m^2$$
 (2.34)

The proposed height of the screen,  $h_{\text{obstacol}}$  was calculated using the relationship:

$$A_{permeabil}^{10\%} = (h_{tunel} - h_{ecran}) \times l_{tunel} + h_{ecran} \times l_{tunel} \times A_{liber\check{a}}$$
 (2.35)

From the equation it follows that  $h_{\text{ecran}} = 50$  mm, corresponding to a screen with the dimensions of 400 mm x 50 mm consisting of a screen with wire diameter d = 0.08 mm and the length and width of the gap  $d_{ochi} = 0.13$  mm.

After determining the height of the screen, its total area was calculated:

$$A_{ecran} = l_{ecran} \times h_{ecran} = 0.02m^2 \tag{2.36}$$

The total permeability of the screen was calculated with the formula:

$$\sigma_{liber} = A_{liber\check{a}} \times A_{obstacol} = 0.012m^2 \tag{2.37}$$

And the blocked area of the protective screen was calculated by subtracting from the total area of the  $A_{ecran}$  screen its permeability  $\sigma_{liber}$ .

$$\sigma_{blocat} = A_{ecran} - \sigma_{liber} = 0.008m^2 \tag{2.38}$$

Knowing these values, the necessary parameters for modeling the screen were calculated in the numerical modeling program COMSOL Multiphysics<sup>TM</sup>, starting with its solidity:

$$\sigma_s = \frac{\sigma_{blocat}}{A_{ecran}} = 0,42 \tag{2.39}$$

The resistance of the protective screen, calculated according to the previously mentioned formula (2.30):

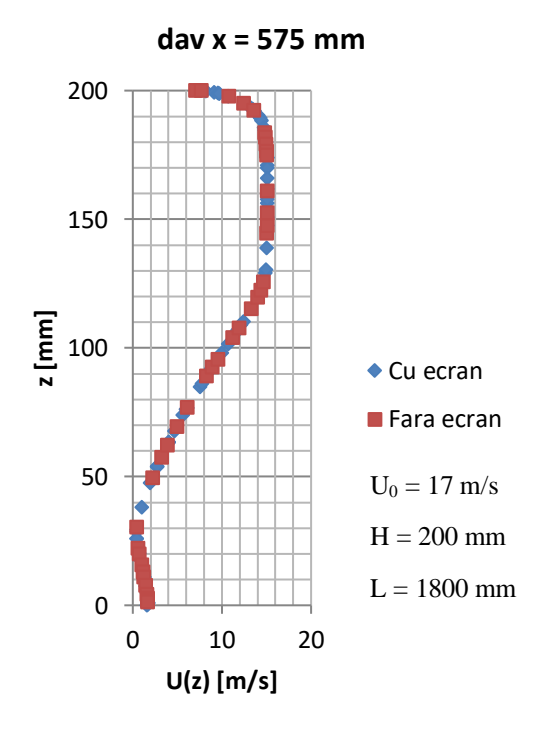
$$K = 0.98 \times ((1 - \sigma_s)^{-2} - 1)^{1.09} = 2.00 \tag{2.40}$$

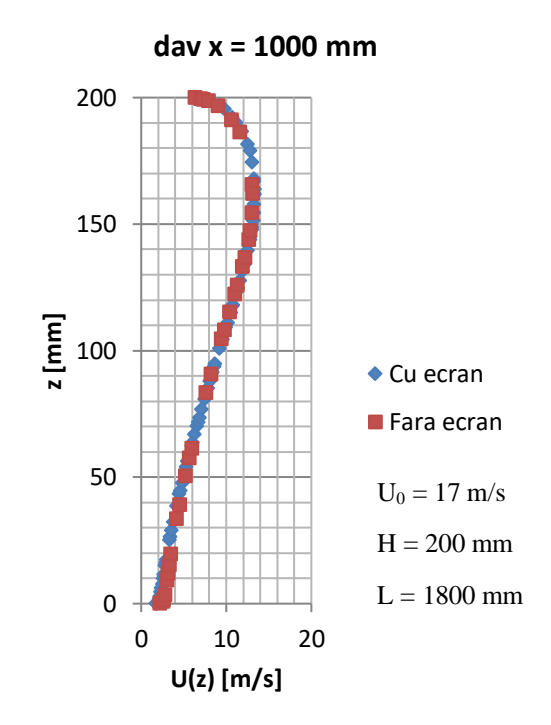
The refractive index, calculated according to the previously mentioned formula (2.31):

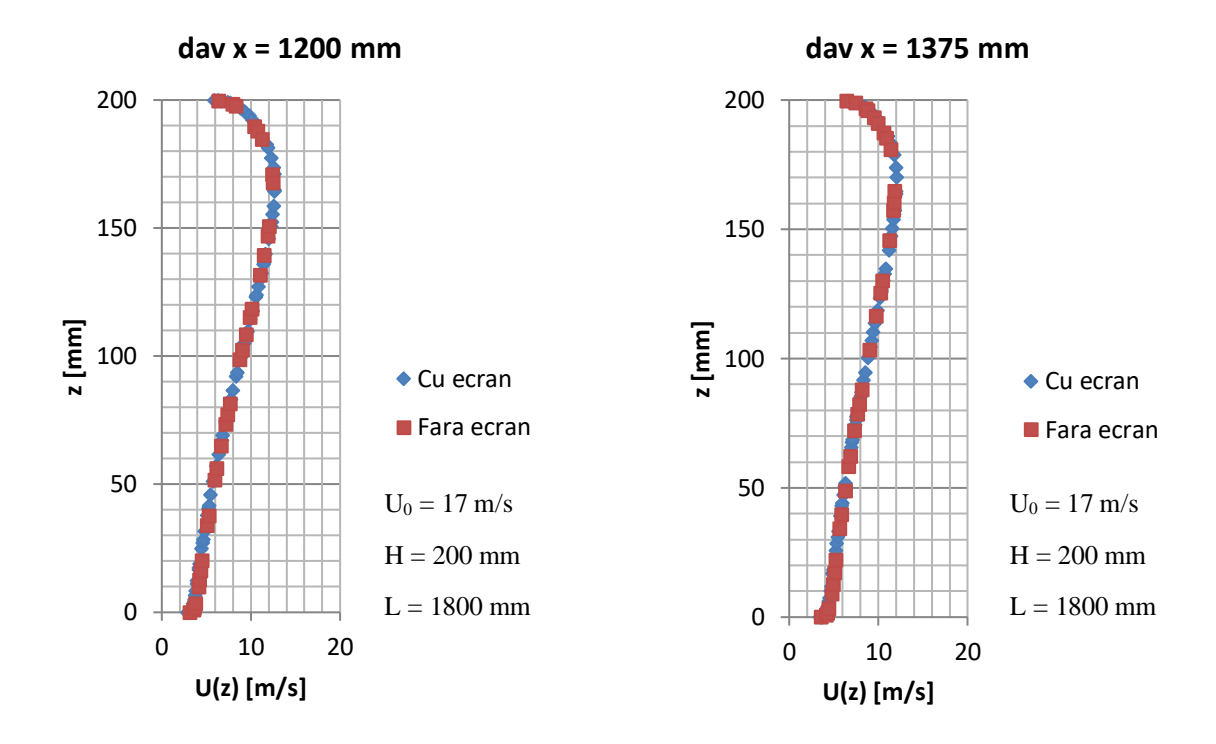
$$\eta = \sqrt{\frac{K^2}{16} + 1} - \frac{K}{4} = 0.62 \tag{2.41}$$

After performing the numerical simulation, the speed graphs related to the 575, 1000, 1200 and 1375 mm sections were created. The protective screen itself was inserted at a distance from the entrance to the experimental vein of 900 mm.

## 2.5.1.1 Comparison of average velocity profiles in $x=575,\,1000,\,1200,\,1375$ mm sections of the TAD vein, with protective shield, obtained by COMSOL k- $\epsilon$ numerical simulation and without screen







#### **Results:**

It can be seen that in the immediate vicinity of the section where the protective screen was inserted the speed decreases, namely in the profiles related to the section x = 1000 mm.

### 3. NUMERICAL TESTS FOR WIND EROSION REDUCTION SOLUTIONS UNDER THE ACTION OF THE WIND

### 3.1 NUMERICAL MODELING OF AIR MOVEMENT OVER SANDY SOIL PROVIDED WITH PROTECTIVE SCREENS

In the research conducted in the previous research report, the numerical simulations k -  $\epsilon$  in the finite element modeling program COMSOL Multiphysics were compared with the results of experimental tests performed in the same wind tunnel with expansion stage. In this case, too, the COMSOL numerical simulations led to very close results, in terms of speed profiles, with the experimental tests, thus considering the numerical model as being experimentally validated.

Due to this fact, it was considered that the numerical treatment of the studied problems and therefore the afferent numerical tests, can be solved, with a very good approximation, by using the finite element modeling method COMSOL Multiphysics.

In the numerical simulations the inlet boundaries were entered as incident speed profiles, the results of previous calculations, with the power law, for the speeds at the reference height U(10) = 8 m/s, U(10) = 12 m/s and U(10) = 16 m/s. These 3 incident wind speed profiles are shown graphically in the following figures.

Figure 3.1.1 shows the speed profile of the incident wind upstream of the protection screens for the exponent  $\alpha = 0.16$  and the reference speed U(10) = 8 m/s.

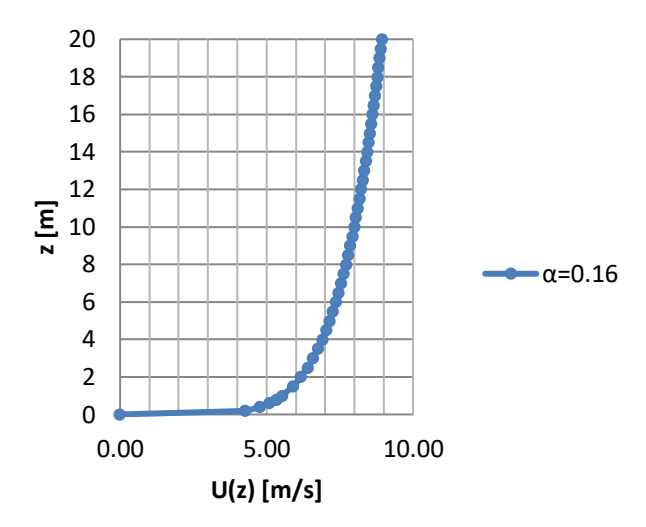


Fig. 3.1.1 - The incident wind speed profile upstream of the protection screens for the exponent  $\alpha = 0.16$  and the reference speed U(10) = 8m/s

Figure 3.1.2 shows the speed profile of the incident wind upstream of the protection screens for the exponent  $\alpha = 0.16$  and the reference speed U (10) = 12 m/s.

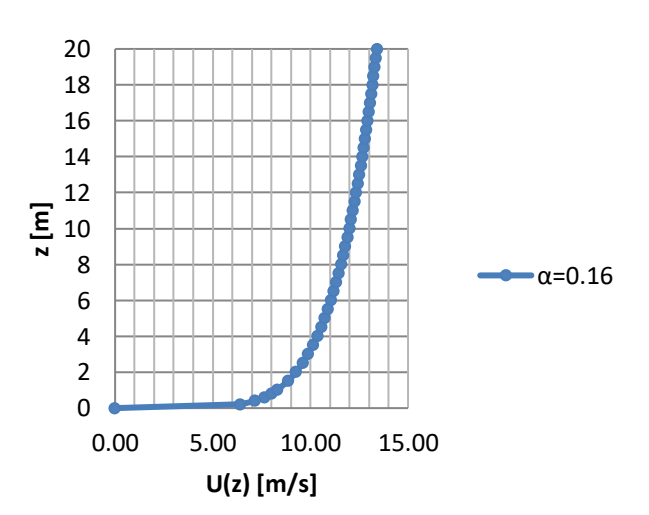


Fig. 3.1.2 - The incident wind speed profile upstream of the protection screens for the exponent  $\alpha = 0.16$  and the reference speed U(10) = 12 m/s

Figure 3.1.3 shows the speed profile of the incident wind upstream of the protection screens for the exponent  $\alpha = 0.16$  and the reference speed U(10) = 16 m/s.

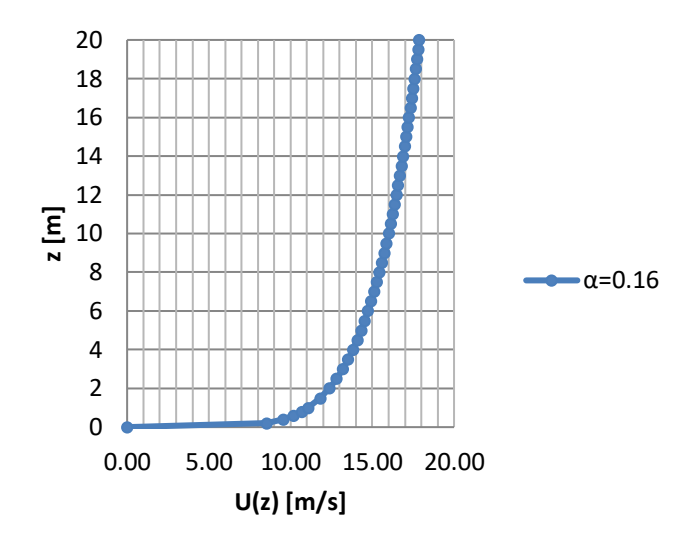


Fig. 3.1.3- The incident wind speed profile upstream of the protection screens for the exponent  $\alpha = 0.16$  and the reference speed U(10) = 16 m/s

#### 3.2 RESULTS OF NUMERICAL SIMULATIONS

In this chapter, the numerical tests performed for 3 reference speeds of the incident wind are presented (U(10)=8 m/s, U(10)=12 m/s, U(10)=16 m/s), for 4 types of protection screens (n=1, 2, 3, 4 screens) and for 4 downstream sections of the screens ( $d_{av}=2H$ ,  $d_{av}=4H$ ,  $d_{av}=6H$ ,  $d_{av}=8H$ ).

#### 3.2.1 Numerical testing for test category CT1 (U(10)=8m/s)

### 3.2.1.1 Numerical testing for the test group GT1,3 (n=3 screens) from the tests category CT1 (U(10)=8 m/s)

These numerical tests were performed for the situations included in the group of numerical tests GT1,3 which refer to the movement of air over a sandy soil provided with 3 rows of permeable protective screens. (n=3), group belonging to the category of numerical tests CT1 relating to a reference speed upstream of the protection screen (U(10)=8 m/s).

The calculation range corresponding to the GT1,3 numerical test group has a length of 100 m (10H) and a height of 20 m. At a distance of 2H = 20 m from the section entering the calculation range there is a protection screen with permeability of 40% and with height H = 10 m.

Figure 3.2.1 shows the diagram of the calculation range in the range of motion for the case of the location of n = 3 protection screens (CT1, GT1,3, CB:40-10-4-2H).

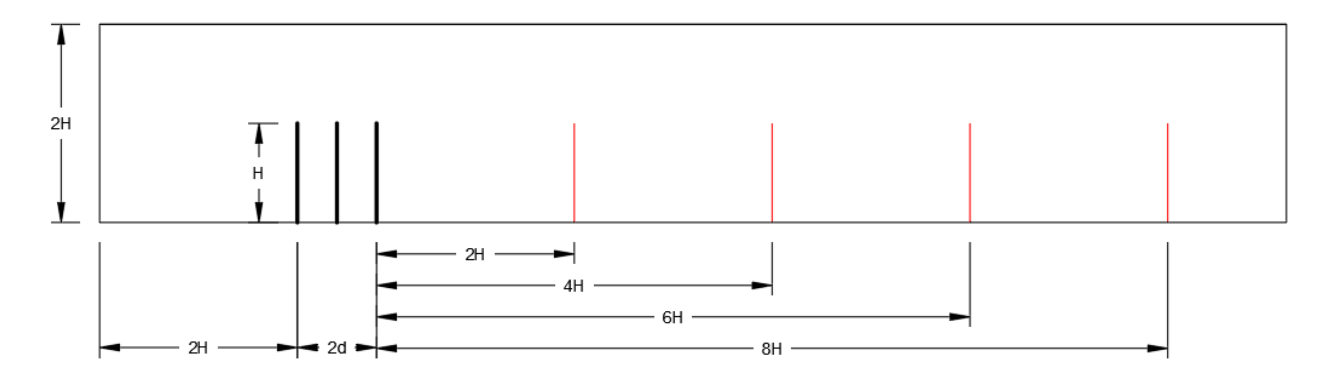


Fig. 3.2.1 – Schematic of the computational domain for the case of placing n=3 protection screens (CT1, GT1,3, CB:40-10-4-2H)

The calculation domain from the computational domain thus established, was then meshed, generating the computing network for calculations, with the COMSOL Multiphysics program at a level of discretization that ensures the obtaining of a speed field, on the range of motion, with a convenient approximation.

Figure 3.2.2 shows the discretization of the computational domain in the area of the protection screens, for a number of protection screens n=3 (CT1, GT1,3, CB:40-10-4-2H).

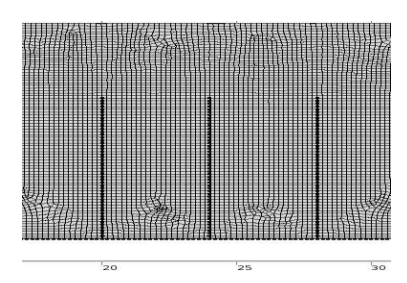


Fig. 3.2.2 - Discretization of the computational domain in the area of the protection screens, for a number of protection screens n=3 (CT1, GT1,3, CB:40-10-4-2H)

Applying, on the computational domain, the finite element model COMSOL Multiphysics, the velocity range in this calculation field is obtained.

Figure 3.2.3 shows the speed field in the computational domain for the reference speed U(10)=8 m/s and number of protection screens n=3 (CT1,GT1,3, CB:40-10-4-2H).

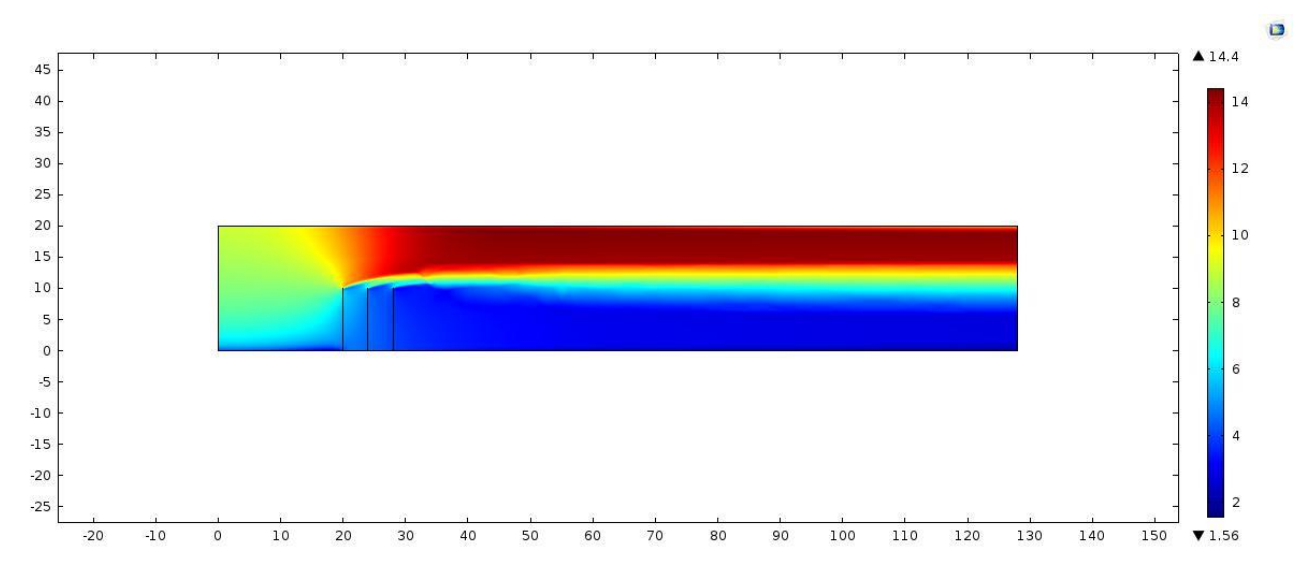


Fig. 3.2.3 - Speed field in the computational domain for the reference speed U(10)=8 m/s and number of protection screens n=3 (CT1,GT1,3, CB:40-10-4-2H)

From the speed field corresponding to the test group GT1,3, from the category of tests CT1, the speed profiles from 4 sections located at the downstream distances from the protection screens were extracted,  $d_{av} = 2H$ ,  $d_{av} = 4H$ ,  $d_{av} = 6H$ ,  $d_{av} = 8H$ . These speed profiles were represented up to the height z = 10 m, because, for the present research, only the speeds at heights  $z_1 = 0.20$  m,  $z_2 = 1.00$  m and  $z_3 = 2.00$  m are concerned, heights at which the phenomenon of sand entrainment produces.

The speed profiles in the 4 sections downstream of the protection screens ( $d_{av} = 2H$ ,  $d_{av} = 4H$ ,  $d_{av} = 6H$ ,  $d_{av} = 8H$ ), resulting from the reduction of the incident wind speed, were compared with the power law type speed profile in upstream of the protection screens, i.e. at heights  $z_1 = 0.20$  m,  $z_2 = 1.00$  m and  $z_3 = 2.00$  m.

Figures 3.2.4, 3.2.5, 3.2.6, 3.2.7 show the speed profiles U(z) downstream of the screens, for the reference speed U(10)=8 m/s and number of protection screens n=3, at distances dav=2H (CT1, GT1,3, TN1,3,1, CB: 40-10-4-2H, CT:8-3-2H),  $d_{av}=4H$  (CT1, GT1,3, TN1,3,2, CB:40-10-4-2H, CT:8-3-4H), dav=6H (CT1, GT1,3, TN1,3,3, CB:40-10-4-2H, CT:8-3-6H), dav=8H (CT1, GT1,3, TN1,3,4, CB:40-10-4-2H, CT:8-3-8H), compared to the speed profile of the incident wind.

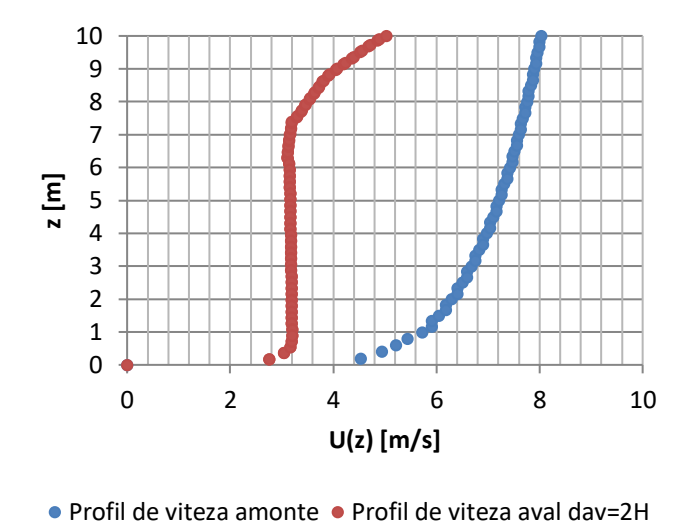


Fig. 3.2.4 - Speed profile U(z) downstream of the screens, for reference speed U(10)=8m/s and number of protection screens n=3, at distance dav= 2H (CT1,GT1,3, TN1,3,1,CB:40-10-4-2H, CT:8-3-2H). Comparison with the incident wind speed profile

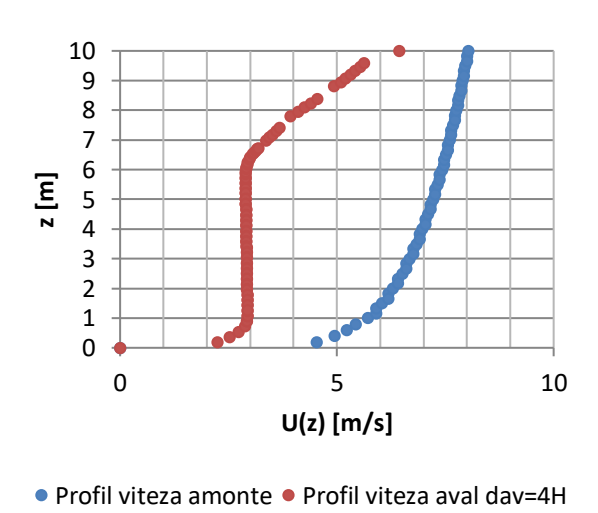
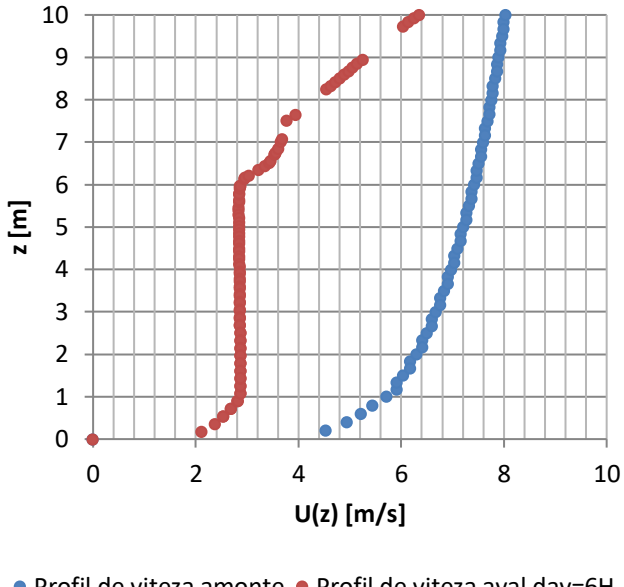


Fig. 3.2.5 - Speed profile U(z) downstream of the screens, for reference speed U(10)=8m/s and number of protection screens n=3, at distance dav= 4H (CT1,GT1,3, TN1,3,2,CB:40-10-4-2H, CT:8-3-4H). Comparison with the incident wind speed profile.



• Profil de viteza amonte • Profil de viteza aval dav=6H

Fig. 3.2.6 - Speed profile U(z) downstream of the screens, for reference speed U(10)=8m/s and number of protection screens n=3, at distance dav= 6H (CT1,GT1,3, TN1,3,3, CB:40-10-4-2H, CT:8-3-6H). Comparison with the incident wind speed profile.

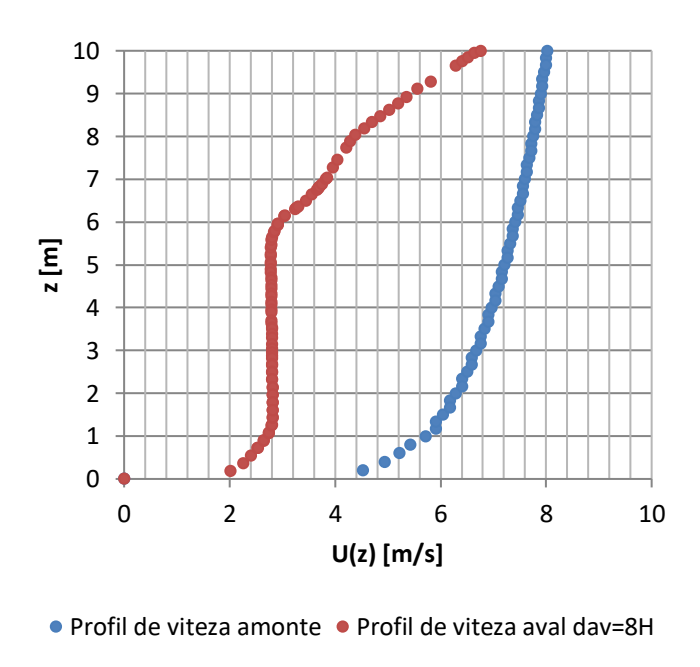


Fig. 3.2.7 - Speed profile U(z) downstream of the screens, for reference speed U(10)=8m/s and number of protection screens n=3, at distance day= 8H (CT1,GT1,3, TN1,3,4,CB:40-10-4-2H, CT:8-3-8H). Comparison with the incident wind speed profile.

Next, wind speeds were determined at heights  $z_1$ =0,20 m,  $z_2$ =1,00 m si  $z_3$ =2,00 m from the speed profiles corresponding to the downstream sections of the protection screens located at distances  $d_{av}$ =2H,  $d_{av}$ =4*H*,  $d_{av}$ =6*H*,  $d_{av}$ =8*H*.

Figure 3.2.8 shows the variation of U speeds at heights  $z_1$ =0,20m,  $z_2$ =1m şi  $z_3$ =2m, depending on the downstream distance  $d_{av}$  for the reference speed U(10)=8 m/s and number of protection screens n=3 (CT1, GT1.3, CB:40-10-4-2H).

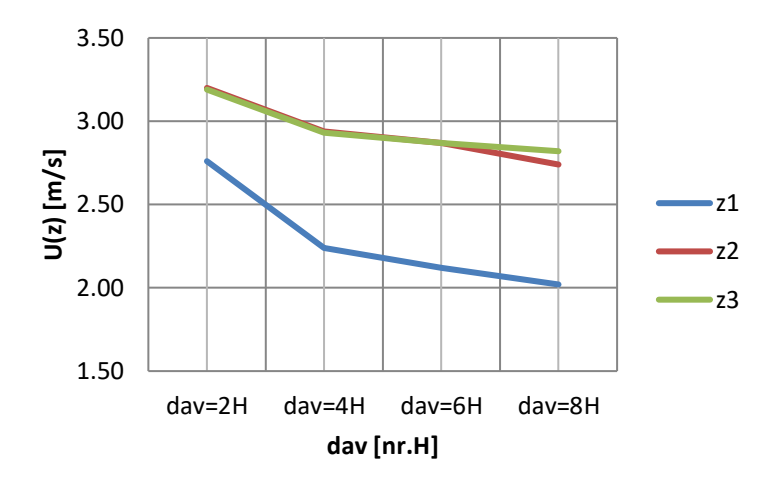


Fig. 3.2.8 - Variation of U speeds at heights z1=0,20m, z2=1m şi z3=2m, depending on the downstream distance day for the reference speed U(10)=8 m/s and number of protection screens n=3 (CT1,GT1,3, CB:40-10-4-2H)

Then, for heights  $z_1$ =0,20 m,  $z_2$ =1,00 m și  $z_3$ =2,00 m, for the sections downstream of the protection screens located at distances  $d_{av}$ =2H,  $d_{av}$ =4H,  $d_{av}$ =6H, $d_{av}$ =8H, the differences were made between the speeds on the upstream speed profile located at  $d_{am}$ =2H and the speeds from the homologous points on the downstream speed profiles, ie  $\Delta U$ =U(z)am-U(z)av.

Figure 3.2.9 shows the variation of the speed decrease  $\Delta U = U(\mathbf{z})\mathbf{am} - U(\mathbf{z})\mathbf{av}$  at the heights  $z_1 = 0.20$ m,  $z_2 = 1$ m și  $z_3 = 2$ m, depending on the downstream distance  $d_{av}$  for the reference speed U(10) = 8 m/s and number of protective screens n = 3 (CT1, GT1,3, CB:40-10-4-2H).

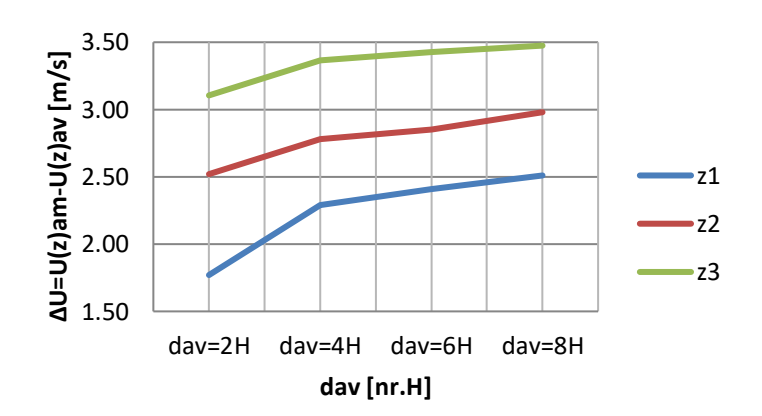


Fig. 3.2.9 - Variation of  $\Delta U=U(z)$ am-U(z)av speeds at heights z1=0,20m, z2=1m și z3=2m, depending on the downstream distance day for the reference speed U(10)=8 m/s and number of protection screens n=3 (CT1,GT1,3, CB:40-10-4-2H)

#### 3.4. CONCLUSIONS REGARDING THE NUMERICAL TESTS

In view of the results of the numerical simulations represented graphically in the paragraphs of Chapter 3, a number of conclusions can be drawn as follows.

From the graphs presented in Chapter 3, it is noted that, in terms of ground speed, denoted by  $U(z_1)$ , it decreases with increasing distance downstream of the protective screens, denoted by  $d_{av}$ .

Considering the minimum sand entrainment speed at ground level,  $U(z_1)_{minantr}$ , as 4 m/s, depending on this speed two tables were made, namely table 4.1 showing the effect of wind at ground level depending on the number of screens, of the reference speed and the downstream distance for  $U(z_1) < 4$  m/s and table 4.2 showing the effect of wind at ground level according to the number of screens, the reference speed and the downstream distance for  $U(z_1) > 4$  m/s

This minimum sand entrainment speed at ground level,  $U(z_1)_{minantr}$ , was established based on Molinkov's study, presented in the work of Moţoc M. from 1963. In this study it is shown that at speeds between 0.5 m/s and 4 m/s the wind at ground level does not lift the sand granules, at speeds between 4 m/s and 7 m/s it drives sand granules with a diameter below 0.5 mm, at speeds between 7 m/s and 11 m/s entrain sand granules with a diameter between 0,5 mm and 1 mm, at speeds between 11 m/s and 17 m/s entrain sand granules with a diameter between 1 mm and 2 mm, and at speeds between 17 m/s and 28 m/s drive sand granules with a diameter between 2 mm and 5 mm.

Table 3.4.1. - Efectul vântului la nivelul solului funcție de numărul de ecrane de protecție, de viteza de referință și de distanța aval pentru  $U(z_1) < 4$  m/s

Number of screens - n	Reference speed – U(10) [m/s]	Downstream distance - $d_{av}$ [nr. $H$ ]	The effect of wind at the ground level – at		
			<b>Z</b> 1		
n = 1 screen	U(10) = 8  m/s	$d_{\mathrm{av}} = 4H$ - $8H$	Does not entrain sand-		
			$U(z_1) \le 4 \text{ m/s}$		
n=2 screens	U(10) = 8  m/s	$d_{\mathrm{av}} = 0H$ - $8H$	Does not entrain sand -		
			$U(z_1) < 4 \text{ m/s}$		
n = 3 screens	U(10) = 8  m/s	$d_{\mathrm{av}} = 0H$ - $8H$	Does not entrain sand -		
			$U(z_1) < 4 \text{ m/s}$		
	U(10) = 12  m/s	$d_{\mathrm{av}} = 0H$ - $8H$	Nu antreneazănisip-		
			$U(z_1) < 4 \text{ m/s}$		
n = 4 screens	U(10) = 8  m/s	$d_{\mathrm{av}} = 0H$ - $8H$	Does not entrain sand -		
			$U(z_1) < 4 \text{ m/s}$		
	U(10) = 12  m/s	$d_{\mathrm{av}} = 0H$ - $8H$	Does not entrain sand -		
			$U(z_1) < 4 \text{ m/s}$		

Table 3.4.2 - Effect of wind at ground level depending on the number of screens, the reference speed and the downstream distance for U(z1) > 4 m/s

Number of screens - n	Reference speed – $U(10)$ [m/s]	Downstream distance $d_{av}$ [nr. $H$ ]	The effect of wind at the ground level – at
			<b>Z</b> 1
n = 1 screen	U(10) = 8  m/s	$d_{\mathrm{av}} = 0H$ - $4H$	Entrains sand under 0,5
			mm -
			$U(z_1) > 4 \text{ m/s}$
	U(10) = 12  m/s	$d_{\mathrm{av}} = 0H$ - $8H$	Entrains sand under 0,5
			mm -
			$U(z_1) > 4 \text{ m/s}$
	U(10) = 16  m/s	$d_{\mathrm{av}} = 0H$ - $8H$	Entrains sand under 0,5
			mm -
			$U(z_1) > 4 \text{ m/s}$
n = 2 screens	U(10) = 12  m/s	$d_{\mathrm{av}} = 0H$ - $8H$	Entrains sand under 0,5
			mm -
	*****		$U(z_1) > 4 \text{ m/s}$
	U(10) = 16  m/s	$d_{\mathrm{av}} = 0H$ - $8H$	Entrains sand under 0,5
			mm -
			$U(z_1) > 4 \text{ m/s}$
n = 3 screens	U(10) = 16  m/s	$d_{\mathrm{av}} = 0H$ - $8H$	Entrains sand under 0,5
			mm -
			$U(z_1) > 4 \text{ m/s}$
n = 4 screens	U(10) = 16  m/s	$d_{\mathrm{av}} = 0H$ - $8H$	Entrains sand under 0,5
			mm -
			$U(z_1) > 4 \text{ m/s}$

Numerical tests have shown that protection against sand entrainment, through screens, at different speeds of the incident wind, takes place in the following situations:

- 1. For U(10) = 8 m/s:
- n = 1 screen, protection is provided at downstream distances day = 4H 8H,
- n = 2 screens, protection is provided at downstream distances day = 0H 8H,
- n = 3 screens, protection is provided at downstream distances day = 0H 8H,
- n = 4 screens, protection is provided at downstream distances day = 0H 8H.
- 2. For U(10) = 12 m/s:
- n = 3 screens, protection is provided at downstream distances day = 0H 8H,
- n = 4 screens, protection is provided at downstream distances day = 0H 8H.
- 3. For U(10) = 16 m/s no group of screens n = 1, 2, 3, 4 provides protection against sand entrainment.

Therefore, for n = 1 screen and n = 2 screens, at wind speeds U(10) = 12 m/s and U(10) = 16 m/s, the wind at ground level ( $U(z_1) > 4$  m/s) entrain sand below 0.5 mm, and for n = 3 screens and n = 4 screens, at wind speeds, U(10) = 16 m/s, wind at ground level ( $U(z_1) > 4$  m/s) entrain sand below 0.5 mm. To reduce the speed at ground level in the cases of sand entrainment presented above, action can be taken by increasing the number of permeable protective screens or by decreasing the permeability of the protective screens, whether natural or artificial.

Also from the graphs presented in Chapter 3, it is noted that, in terms of velocities at the levels  $z_1$ =1 m and  $z_2$ =2 m above the ground, denoted by  $U(z_2)$  and  $U(z_4)$ , respectively, they decrease with increasing downstream distance from the protection screens, denoted by  $d_{av}$ . These two speeds, which are approximately equal, vary depending on the  $d_{av}$ , with values between 0.1 m/s and 0.8 m/s, as shown in Table 4.3.

Test categories	CT1			CT2			СТ3					
Test groups	GT											
	1,1	1,2	1,3	1,4	2,1	2,2	2,3	2,4	3,1	3,2	3,3	3,4
$[U(z_2)=U(z_3)]$ la $d_{av}=2H$ - $[U(z_2)=U(z_3)]$ la $d_{av}=8H$	0,10	0,15	0,20	0,40	0,25	0,30	0,60	0,60	0,30	0,40	0,80	0,60
	m/s											

Table 3.4.3. - Speed variation for  $U(z^2)$  and  $U(z^3)$  between day=2H and day=8H

The numerical research carried out in this doctoral thesis, with the aim of tracking the protection against the phenomenon of sand entrainment from areas with sandy lands, under the action of natural wind, through the use of equivalent natural or artificial protective screens, highlighted the fact that, for a good fraction of the wind speeds and for most of the screen assemblies chosen for the study, a strong decrease in wind speed was obtained downstream of the screens, to the level where the air current no longer entrains sand.

Therefore, based on the results obtained in the present thesis, it is possible to achieve a very good protection of sandy lands from the phenomenon of sand being driven by the wind by placing, in the direction of the dominant wind, natural protective screens (protective forest curtains) or artificial protective screens with equivalent permeability coefficients. The number of protective screens and their dimensions will be established based on the results of the numerical tests carried out in this doctoral thesis.

### 4. CONTRIBUTIONS OF THE THESIS TO THE FIELD OF WIND ENGINEERING

The aim of this thesis is, mainly, to study the possibility of significantly reducing the erosion of sandy soils by using permeable protective obstacles to reduce the speed of the incident wind, studies carried out by numerical methods performing a series of numerical simulations of specific phenomena both on a small scale and on a natural scale, using different permeable obstacles (natural obstacles consisting of forest curtains or artificial obstacles consisting of equivalent mesh screens).

This doctoral thesis is organized into four chapters that present the way in which the entrainment and transport of sand particles is carried out under the action of wind speed and, above all, the numerical simulations regarding ways to reduce this phenomenon.

Chapter 1, entitled *Analysis of the environmental characteristics in areas with sandy soil*, addresses the economic and socio-economic problem of soil degradation, at an international level, presenting certain areas affected by wind erosion, from a historical and geographical point of view, but also areas in Romania that have suffered and/or are suffering from this phenomenon

Also, in this first chapter, the three ways of entrainment of particles are presented mathematically, namely rolling, jumping or suspension, and a study presenting the values of the entrainment speed of sand particles depending on the diameter of the grains they entrain, which was the basis of the results sought in the simulations in the following chapters by looking for obstacles for which the reduction of the speed downstream of them, in the terrain area, will be up to a speed below the allowed upper limit speed of 4 m/s.

Following the establishment of the solution to reduce the wind speed near the ground to below 4 m/s, by using permeable obstacles, the next step was carried out, namely the presentation of a simplified calculation model in which the numerical simulation method used is briefly described in the following chapters, the desired result being that of reducing the speed below the previously mentioned imposed limit, downstream of the group of permeable obstacles.

Chapter 2, entitled Numerical simulation of air movement in the presence of some obstacles of the type of protective screens with different degrees of permeability, presents a series of numerical simulations of air movement in the presence of obstacles with different degrees of permeability and begins with an introduction to turbulence scales and the calculation method of them, focusing on the Kolmogorov length scale

Following the dimensioning of the calculation cell, two numerical simulations of experimental tests performed in the Wind Tunnel with Discontinuity were carried out for which there were data related to the velocity profile in nine distinct sections of the blower. One simulation was performed using ANSYS Fluent finite element modeling program and another simulation was performed in COMSOL Multiphysics program.

After calibrating the numerical model, a series of permeable obstacles were introduced downstream of the entrance to the computational domain to reduce the downstream velocity to an admissible velocity below 4 m/s in the area closest to the ground.

The results showed that, by placing the permeable obstacles successively and with variable heights, increasing from small to large and from large to small, the speed downstream of them was reduced below the permissible limit value of 4 m/s.

Both the results obtained and presented and the calibration of the numerical model were the basis for the preparation of **chapter 3** called *Numerical tests for wind erosion reduction solutions under the action of the wind*, in which a series of numerical simulations were carried out in the finite element modeling program COMSOL Multiphysics, at natural scale, for a computational domain of 20 m height and 120 m length, for different reference wind speed categories (U(10) = 8 m/s, 12 m/s, 16 m/s) and for different protection groups characterized by the number of protection screens (n=1, 2, 3, 4 screens)

Since a total of 48 numerical simulations were performed for 3 reference wind speeds, for 4 types of shield assemblies and for 4 sections downstream of the shield group, they were coded for ease of identification of the respective tests.

At the end of the simulations, the research conclusions were drawn in **sub-chapter 3.4** called *Conclusions regarding the numerical tests*, in which the situations in which, by using permeable obstacles, the speed downstream of them drops below the upper limit speed of 4 m/s, and within **chapter 4**, named *Contributions of the thesis to the field of wind engineering*, the contributions of this

doctoral thesis in the field of wind engineering were identified with the pursuit of the phenomenon of stopping the erosion of sandy soils through the use of equivalent artificial permeable obstacles, through the degree of permeability, natural forest curtains

The doctoral thesis *Numerical contributions regarding the interaction of wind with permeable obstacles for the protection of sandy soils* contains a series of contributions, which were highlighted and developed throughout the doctoral internship. The most important contributions, numbered **C1**, **C2**, **C3**, **C4** and **C5** refer to:

#### C.1. Optimal computational cell sizing for motion domain discretization

This involved a series of stages, each with a contributing character:

#### C.1.1. Use of two calculation methods for sizing the calculation cell

In order to avoid overcrowding the computational process of solving the simulation in the first phase, two calculation methods were used for the dimensioning of the calculation cell for discretization. The first method is based on Kolmogorov's theory and the second method is based on the Turbulent Kinetic Energy - TKE turbulence model.

#### C.1.2. Making a maximum and minimum range when choosing the size of the calculation cell

In the second phase, the size of the calculation cell, resulting from calculations using the two methods, was increased by 6 to 30 times for both results. This is to achieve a maximum and minimum cell range in order to choose the optimal calculation cell size to prevent DNS simulation from occurring.

#### C.1.3. Choosing the optimal size of the calculation cell

After obtaining the results, the size of the cell was chosen taking into account that its value can be found on both the maximum and minimum intervals regardless of the calculation method used, and that the size of the calculation cell has a value that is validated by both calculation methods.

This can be considered as an effective strategy for establishing the minimum and maximum dimensions of the finite elements for the discretization of the computational domain so as to facilitate the solution process of various numerical simulations carried out with the help of specialized programs.

### C.2. Validation (calibration) of the numerical model with the experimental one using RANS and LES numerical simulations

This involved a series of stages, each with a contributing character:

#### C.2.1. Realization of a numerical model of TAD

After sizing the calculation cell, a full-scale numerical model of the wind tunnel with discontinuity (TAD) and a physical experiment carried out in it was made, for which data on the resulting velocity profiles in certain sections of the tunnel were available. Numerical simulations were performed with two distinct programs, COMSOL Multiphysics finite element calculation and ANSYS Fluent finite volume calculation.

#### C.2.2. Simulation with COMSOL-k-E and with ANSYS-LES

Due to the different computational calculation methods of the two programs, the simulation with COMSOL Multiphysics was performed using the k- $\varepsilon$  method, and the simulation with ANSYS Fluent was performed using the LES method.

#### C.2.3. Validation of numerical tests based on experimental tests

In both simulations, results similar to those obtained from the physical experiment were obtained, so that, by correctly simulating the phenomenon of air flow in the experimental vein, it was possible to validate the obtained results.

This was materialized by making graphs comparing the velocity profiles for the physical experiment and for the two numerical simulations in the same sections of the tunnel, mentioned previously.

### C.3. Creation of a numerical model of air flow over a series of permeable screens based on the previously validated model

This involved a series of stages, each with a contributing character:

### C.3.1. Realization of a COMSOL numerical model on a full-scale model of air flow over a sandy terrain

After matching the numerical model with the experimental one, a new series of simulations was carried out in the COMSOL Multiphysics program, this time on a full-scale model, which simulates the flow of air over a sandy soil, susceptible to erosion.

The model consists of a calculation domain 20 m high and 120 m long to which 4 m have been added, the distance between two successive permeable screens, the screens having a height of 10 m.

#### C.3.2. Simulating an erosion-sensitive terrain

The considered condition for the land studied in the simulation to behave as a land sensitive to erosion is that the entrainment of the sand particles in the laminar boundary substrate band will be achieved for a velocity in the immediate vicinity of the ground of more than 4 m/s.

This value of the minimum sand entrainment speed at ground level was established based on Molinkov's study, presented in the work of Moţoc M. from 1963.

### C.4. Performing a series of air flow simulations over a series of permeable screens at a reference wind of various speeds

This involved a series of stages, each with a contributing character:

#### C.4.1. Establishing the average reference wind speed profiles

Starting from the premise of knowing the value of the reference wind speed U(10) = 8 m/s, 12 m/s and 16 m/s, three graphs were made for the variation of the related speed field, which were used to introduce of the incident wind in the calculation section.

### C.4.2. Performing numerical tests for one, two, three or four permeable screens and a reference wind of different speeds

Thus, 3 categories of tests were carried out, each consisting of one, two, three or four permeable screens.

Four simulations were carried out for each case of the reference wind, depending on the number of permeable screens located downstream of the entrance section of the calculation domain, following the vertical distributions of the speed in 4 sections located downstream of the group of screens permeable protection. Following the simulations, graphs were made for the values of the velocity field in order to observe in which situations the velocity in the laminar boundary substrate strip decreases or exceeds the reference value of 4 m/s.

### C.5. Identifying cases where the velocity downstream of one or more permeable obstacles falls below the particle entrainment velocity

After making the graphs with the values of the velocity fields downstream of the permeable screens, the situations were identified and selected for which the placement of one or more screens reduces the air speed downstream of them below the upper limit speed of 4 m/s.

This helps to better understand the phenomenon of erosion of sandy soils located downstream of one or more permeable screens and implicitly in establishing solutions for the choice and placement of these screens in the wind path affecting areas sensitive to the entrainment of sand particles from the studied areas.

#### **SELECTIVE BIBLIOGRAPHY**

- [1]. Lupe I., Influența perdelelor forestiere asupra umezelii solului. (Analele ICAS, 12 (1): 217–234, 1951.).
- [2]. Traci C., Împadurirea terenurilor degradate. (Ed. Ceres, București, Romania, 1985).
- [3]. Neşu I., Perdele forestiere de protecție a câmpului (Editura Star Tipp. Slobozia, Romania 1999).
- [4]. Nuță S., Caracteristici structurale și funcționale ale perdelelor forestiere de protecție a câmpului agricol din sudul Olteniei. (Analele ICAS, 48:161–169, 2005).
- [5]. Costăchescu C., Dănescu F., Mihăila E., Perdele forestiere de protecție. (Editura Silvică, București, Romania, 2010).
- [6]. Wilcox, D. C., Turbulence Modeling for CFD, Third edition, DCW Industries, (United States of America by Birmingham Press, Inc., San Diego, California, 2006).
- [7]. Vladut C. V., Modelarea numerica si experimentala a miscarilor atmosferice la scara medie peste insula Bolund, (Teza de doctorat, Bucuresti, Romania, 2015)
- [8]. Davenport, A.G., Wind Loads on Structures. (Ottawa: Technical Paper No. 88 of the Division of Building Research, 1960).
- [9]. Moțoc, M., Eroziunea solului pe terenurile agricole și combaterea ei. (Editura Agro-Silvică, Bucuresti, Romania, 1963)
- [10]. Doroftei, B.I., Degeratu, M., Bandoc, G., Iordache, O.G., Moga, C.I., Researches on the use of textile materials for protection against soil erosion, (Industria Textila, nr. 2/2020, pg. 163-167, București, Romania)